NWRI CONTRIBUTION 87-156

SIMULATION OF WIND-INDUCED WATER CURRENTS

by

Ioannis K. Tsanis

Visiting Fellow
Research and Applications Branch
National Water Research Institute
Canada Centre for Inland Waters
867 Lakeshore Road, P.O. Box 5050
Burlington, Ontario, Canada L7R 4A6

August 1987

PERSPECTIVE GESTION

Il est essentiel de comprendre le processus du transfert d'énergie mécanique entre les vents et les courants pour modéliser correctement la circulation et les processus de mélange dus au vent dans les lacs. Des travaux antérieurs portant sur la question sont examinés, une nouvelle méthode de simulation des courants en laboratoire est présentée et une nouvelle solution analytique est vérifiée.

J. Lawrence
Directeur, Recherches et applications

RÉSUMÉ

Ce document passe en revue les méthodes expérimentales théoriques et traditionnelles d'étude des courants produits par le vent et présente une nouvelle méthode de simulation de ces courants en laboratoire. Les profils de vitesse moyenne obtenus dans les ensembles air-eau classiques, quand ils sont établis en fonction des coordonnées de la loi de la distribution des vitesses, placent toutes les expériences dans le domaine de la rugosité transitoire. Les lacunes des ensembles air-eau simulés en laboratoire, tels l'impossibilité de régulariser la rugosité de surface et le caractère tridimensionnel de l'écoulement, sont corrigées par la mise en oeuvre d'une nouvelle méthode expérimentale qui permet de représenter la masse d'eau considérée par le volume d'air contenu dans une boîte qui se déplace et l'interface air-eau par la surface d'un mur fixe. Les profils de la vitesse moyenne produits par cette méthode servent à vérifier une solution analytique fondée sur la distribution parabolique de la viscosité tourbillonnaire.

Simulation of Wind-Induced Water Currents

By Ioannis K. Tsanis, M.ASCE [1]

Abstract: This paper presents a review of theoretical and conventional experimental approaches to studies of wind-induced water currents and introduces a new method for simulating these motions in the laboratory. Mean velocity profiles obtained in conventional air-water systems when plotted in terms of the coordinates of the "smooth inner" law of velocity distribution, delegate all of the experiments into the region of transitional roughness. The shortcomings of laboratory air-water systems such as uncontrollable surface roughness and three-dimensionality of flow are overcome with a novel experimental approach in which the actual water body is represented by the air volume contained inside a moving box, and the surface of a stationary wall constitutes the actual air-water interface. Mean velocity profiles obtained with this apparatus are used to verify an analytical solution based on the parabolic distribution of the eddy viscosity.

Introduction

Turbulent mixing in reservoirs and lakes is primarily caused by wind which is the principal source of the required mechanical energy. The wind acting on the water body surface causes a drift current in the direction it blows thus producing a windward lowering of the water level and a leeward rise, which is called wind set-up (Hellstrom 1979). This tilt of the surface creates a pressure gradient which induces a bottom flow in the opposite direction to that generated by the wind which ensures zero net mass flux in the vertical plane, for 2-D flows only, but not necessarily in lakes of variable bathymetry.

Both field and laboratory experiments may be conducted to study wind effects on water bodies. Although field experiments are most desirable, laboratory experiments are usually preferred because they are less costly, less complicated, and the physical variables can be more readily controlled. The types of flow of interest are

[1] Visiting Fellow, National Water Research Institute, Canada Centre for Inland Waters, Burlington, Ontario, L7R 4A6, Canada.

characterized as "nearly horizontal flows" due to their large horizontal extent and relatively shallow depth. However, the topographical details, i.e., irregularities in depth and plan, and the large number of physical variables involved in actual environmental flows make it very difficult to incorporate all of them in laboratory experiments. Therefore, most model studies of wind-induced water currents are simplified replicas of actual flows, and are executed in laboratory systems combining air and water tunnels.

The existing experimental data were obtained in conventional laboratory air-water tunnels of water depth to width ratio of 1:1 to 1:4. Results obtained in these systems are 3-D on both the air side and the water side of the interface due to side wall friction effects. This leads to velocity profiles at the centre of the experimental facility which have nonzero net mass flux. On the other hand, the analytical models of wind-induced water currents which are based on the previous experimental findings, are all 2-D in nature.

Recognizing the shortcomings of conventional modelling systems, a new approach toward the physical simulation of the wind-induced currents is undertaked and is schematically depicted in Fig. 1. In this approach, the water body is represented by the air volume contained inside the moving bottomless box, and the surface of the stationary bench constitutes the air-water interface. The simplified flow under consideration is homogeneous, 2-D in a vertical plane, comprising a shear-induced current at the exposed surface, and an opposing pressure-driven current near the bottom. Shear is applied directly to the subject fluid volume (air in the present instance) by sliding it relative to a stationary plane surface representing the actual air-water interface. The model overcomes some of the problems plaguing the conventional laboratory systems; (a) the velocity distribution in the transverse direction is essentially uniform because of minimized side-wall effects and, as a result, continuity is preserved better than the conventional models; (b) the ratio of the surface velocity to the surface shear velocity is of the same order of magnitude as the corresponding ratio in the conventional systems; (c) the roughness , i.e., the waviness of the free surface can be controlled; and (d) the hot-wire velocimetry technique can be used for turbulence measurements because the working fluid is air. The present study is restricted to hydrodynamically smooth interface conditions, since the aqueous boundary layer in the field is generally in the hydrodynamically smooth regime (Wu 1973) while in the laboratory it is in the transitionally rough towards the smooth regime (Wu 1975).

A literature review is undertaken considering both the analytical and experimental approaches to the problem. The analytical background for the analysis of wind-induced currents for both the laminar and turbulent case is described. Experimental results of mean velocity profiles obtained in conventional air-water systems are compiled, presented and discussed. Measurements of mean velocity profiles obtained with the new modelling approach are described and compared with ones obtained in the conventional air-water systems and with analytical ones. A simplified distribution law for the vertical eddy viscosity is proposed for application to prototype problems.

Theoretical Background of Shear-induced Flow

Steady Laminar Shear-induced Flow: This flow has a parabolic velocity distribution and a linear shear stress distribution (Hellstrom 1941 & Keulegan 1951). The bottom to surface shear stress ratio $\eta = \tau_b/\tau_s = -0.50$, the shear stress is zero at z/h = 1/3, and the velocity u = 0 occurs at z/h = 0 and z/h = 2/3.

Steady Turbulent Shear-Induced Flow: The applicable equations for this flow are

$$\frac{\partial \bar{u}}{\partial x} = 0; \qquad i.e., \ \bar{u} = \bar{u}(z) \tag{1}$$

$$0 = -\frac{1}{\rho}\frac{\partial \bar{P}}{\partial x} + \nu \frac{d^2\bar{u}}{dz^2} - \frac{d\overline{u'w'}}{dz} \tag{2}$$

$$0 = -\frac{d\overline{v'w'}}{dz} \qquad i.e., \ \overline{v'w'} = \overline{v'w'}(z) \tag{3}$$

$$0 = -\frac{1}{\rho}\frac{\partial \bar{P}}{\partial z} - \frac{\partial \overline{w'^2}}{\partial z} \tag{4}$$

with the boundary conditions

$$\bar{u} = \overline{u'w'} = \overline{v'w'} = 0 \ \ at \ \ z = 0 \ , \ \bar{u} = u_s \ \text{and} \ \overline{u'w'} = \overline{v'w'} = 0 \ \ at \ \ z = h \tag{5}$$

Integration of Eq.(5) with respect to z yields $\bar{P} + \rho\overline{w'^2} = \overline{P_o}(x)$ where $\bar{P}_o$ is the piezometric pressure on the flow boundaries z = 0 and z = h. Accordingly, $\frac{\partial \bar{P}}{\partial x} = \frac{d\overline{P_o}}{dx}$ and integration of Eq. (2) with respect to z yields

$$\frac{d\overline{P_o}}{dx} z = \mu \frac{du}{dz}\Big|_0^z - \rho\overline{u'w'}\Big|_0^z = \tau(z) - \tau_b \tag{6}$$

which describes a linear variation for the total shear stress, (i.e., the sum of viscous and turbulent contributions) in the vertical direction. Close to the flow boundaries at z = 0 and z = h, the viscous stresses are predominant and the Reynolds stresses are negligible. On the other hand, inside of the flow field proper it is the Reynolds stresses which greatly exceed the viscous contribution.

The velocity distribution $\bar{u} = \bar{u}(z)$ follows from a solution of Eq. (2) and depends on the distribution of the turbulent shear stress with z which is provided by introducing appropriate "closure" hypotheses.

Models of Reynolds-stress Distribution, and Resulting Solutions

Various classical closure hypotheses for expressing the turbulent shear stress in terms of the mean velocity are applied to the solution of Eq. (2) which describes the shear-induced flow under consideration.

Boussinesq's Eddy Viscosity: In analogy with laminar flow, the Reynolds stresses are represented as

$$\tau = -\rho \overline{u'w'} = \rho \nu_t \frac{d\bar{u}}{dz} \tag{7}$$

where $\nu_t = \mu_t/\rho$ is the kinematic eddy viscosity which is a property of the flow. A constant over the depth eddy viscosity μ_t leads to a parabolic velocity distribution as in the laminar case. The eddy viscosity is a function of z for the case of turbulent flow. For instance, the assumption of a logarithmic velocity distribution suggests a parabolic distribution of the eddy viscosity over the depth of the flow as demonstrated by Elder (1959) and Lau & Krisnappan (1981) in analytical and numerical studies of turbulent mixing phenomena. Similarly, Pearce & Cooper (1981) used a linearly varying eddy viscosity in their numerical model of wind-induced water currents.

Prandtl's Mixing Length: The mixing length hypothesis, gives the relation between stress and the velocity gradient as follows

$$\tau = \rho\, l_m^2 \left| \frac{d\bar{u}}{dz} \right| \frac{d\bar{u}}{dz} \tag{8}$$

where l_m is the mixing length which is related via Eq. (7) to the eddy viscosity as ($\nu_t = l_m^2 \left| \frac{d\bar{u}}{dz} \right|$). The mixing length, like the eddy viscosity, is a property of the flow and, in first approximation, is supposed to be a purely local function. Reid (1957), in his analytical study of turbulent channel flow subject to surface wind-stress, assumed a parabolic distribution of the mixing length in the vertical. This approach yields a series of solutions for the velocity distribution in terms of different shear-stress ratio. In order to satisfy the continuity requirements, i.e., zero net-mass flux, he found that the shear stress ratio must be equal to $\eta = -0.097$ which is very close to the value of -0.10 or less (Van Dorn 1953).

One-equation, or k–L_o Model of Turbulence: According to this model the turbulent mean velocity could be determined by directly solving the differential transport equation rather than by relying on phenomenological relations such as the ones given by the Eqs. (7) and (8). Introducing the time-averaged turbulent kinetic energy per unit mass, $k = 1/2\,(\overline{u'^2} + \overline{v'^2} + \overline{w'^2})$ in the eddy viscosity concept, results in, $\nu_t = c_t\, k^{1/2}\, L_0$ in which L_o is the dissipation length scale (Rodi 1978). The dissipation ε is usually modelled by the expression $\varepsilon = c_d\, k^{3/2}/L_o$, where c_t and c_d are numerical constants with a value around 0.3 (Koutitas & O'Connor 1981). The form of the equation for turbulent kinetic energy for 2-D nearly horizontal flows at high Reynolds numbers is

$$\frac{Dk}{Dt} - \frac{\partial}{\partial z}\left(\frac{\nu+\nu_t}{\sigma_k}\,\frac{\partial k}{\partial z}\right) - \nu_t\left(\frac{\partial \bar{u}}{\partial z}\right)^2 + c_d\,\frac{k^{3/2}}{L_0} = 0 \tag{9}$$

where σ_k is an effective turbulent Prandtl number with a value approximately equal to unity. The mixing length hypothesis is a special case of the k–L_o turbulence model if both the convective and diffusive transport terms are negligible, in which case $l_m = (c_t^{\,3}/c_d)^{1/4}\, L_o$.

The one-equation model was used for the modelling of wind-induced flows under the assumption of steady and uniform by Koutitas & O'Connor (1981) under the assumption of steady and uniform conditions, i.e., Dk/Dt = 0. With the aid of a complicated expression for the dissipation length scale they arrived at a solution for the eddy viscosity which is described by the following empirical relation $\nu_t = 0.1249\, u_{*s}\, h\, z_h\, (2 - z_h)$ where $u_{*s} = (\tau_s/\rho)^{1/2}$ is the surface shear velocity. This solution is not satisfactorily close to the air-water interface. A modified distribution of the dissipation length scale L_o based on experimental observations solved this inconsistency, and led to an improved distribution of the eddy viscosity over the depth $\nu_t = 0.1249\, u_{*s}\, h\, (1 - z_h)\,(5\, z_h - 1)$.

Two-equation, or k–ε Model of Turbulence: The k–ε model includes an expression for the eddy viscosity and two coupled differential equations for the turbulent kinetic energy k and the dissipation of this energy, ε which for 2-D nearly horizontal flows at high Reynolds numbers are, respectively, (Svensson 1978)

$$\nu_t = c_t\,\frac{k^2}{\varepsilon} \tag{10}$$

$$\frac{Dk}{Dt} = \frac{\partial}{\partial z}\left(\frac{\nu+\nu_t}{\sigma_k}\,\frac{\partial k}{\partial z}\right) + \nu_t\left(\frac{\partial \bar{u}}{\partial z}\right)^2 - \varepsilon \tag{11}$$

$$\frac{D\varepsilon}{Dt} = \frac{\partial}{\partial z}\left(\frac{\nu+\nu_t}{\sigma_\varepsilon}\,\frac{\partial \varepsilon}{\partial z}\right) + c_{1\varepsilon}\,\nu_t\,\frac{\varepsilon}{k}\left(\frac{\partial \bar{u}}{\partial z}\right)^2 - c_{2\varepsilon}\,\frac{\varepsilon^2}{k} \tag{12}$$

in which σ_ε = effective Schmidt number; c_t = numerical constant in eddy viscosity expression; and $c_{1\varepsilon}$ and $c_{2\varepsilon}$ = numerical constants in the dissipation of turbulent kinetic energy equation. The standard k–ε model was used by Svensson (1978) with model constant values $c_t = 0.09$, $\sigma_k = 1.0$, $\sigma_\varepsilon = 1.3$, $c_{1\varepsilon} = 1.44$ and $c_{2\varepsilon} = 1.9$. to calculate a wind-induced channel flow. He considered the free surface as a moving wall at which the shear stress is prescribed and used as the input variables surface shear velocity $u_{*s} = 0.092\, N/m^2$ and the depth $h = 0.30\, m$ from (Baines & Knapp 1965) experiments. He found a surface velocity ratio $\bar{u}_{os} = 22$, a zero mean velocity at the normalized depth $z_h = 0.65$ and a maximum eddy viscosity, normalized by the surface shear velocity u_{*s} and the depth h, of 0.08 at $z_h = 0.55$.

Mean velocity profiles based on the above numerical techniques are presented in nondimensional form in Fig. 2. The calculated, or pre-defined eddy viscosities used in the various numerical models, normalized by the surface shear stress and the channel depth, are depicted in Fig. 3. All the numerical models require knowledge of the surface shear velocity u_{*s} and the depth h. The assumed distribution of eddy viscosity used in the linearly varying eddy viscosity model is based on observations of open channel flow (Pearce & Cooper 1981). In the mixing length model, the vertical distribution of the mixing length is defined empirically, using as a guide the values of this length that successfully described other shear flow experiments (Reid 1957). The shortcoming of this approach is evident that a zero eddy viscosity is yielded at the position of zero mean velocity gradient.

The k–L_e model overcomes this problem. Here the vertical distribution of the dissipation length L_e is predefined based on empirical relations similar to those used for the mixing length. The eddy viscosity is calculated by solving the differential equation for the turbulent kinetic energy. The diffusion effects, represented by the second term on the left-hand-side of Eq. (9), act as a spreading and smoothing mechanism. Thus, discontinuities in the solution are avoided as can be seen in Fig. 3. For this reason the k–L_e model is preferred to the mixing length model in problems related to countercurrent flows. The eddy viscosity based on the modified k–L_e model has been successfully used in calculating the water circulation of the Gulf of Thessaloniki in the Aegean sea of Greece (Ganoulis et al. 1980). The eddy viscosity based on k–ε is calculated by solving the two coupled differential equations for the turbulent kinetic energy and its dissipation. This model is more complex than the other ones but does not require a priori knowledge of the distributions of mixing or dissipation lengths. All of the eddy viscosities based on the foregoing models are mutually consistent in their overall magnitudes, and are in good agreement with those found in open channel flows (Pearce & Cooper 1981).

The analytically predicted velocity profiles compiled in Fig. 2 differ significantly from each other. The reason for this rests in the fact that the constants used in these models are based on experimental findings of varying quality and different theories. For example, Pearce & Cooper (1981) and Svensson (1978) used Baines & Knapp's (1965) experimental results to justify their predictions. Similarly, Reid (1957) used existing experimental results and Koutitas & O'Connor (1981) used their experimental results to justify their predictions. Furthermore, there is always some scatter in the experimentally measured mean velocities. Reasons for this include the 3-D nature of conventional laboratory flows, the possibility that the flows are not fully developed, and the difficulties in measuring velocities close to a wavy surface.

A New Analytical Solution for Turbulent Shear-induced Flow

The concept of eddy viscosity is used to describe the Reynolds stresses. In order to calculate the velocity distribution in turbulent flow, it is necessary to specify a vertical distribution of the eddy viscosity. A parabolic distribution in the vertical suggested by an anticipated logarithmic velocity profile in previous studies, yields the following algebraic form for the kinematic eddy viscosity

$$\nu_t = \frac{\lambda\, u_{*_s}}{h}\,(z + z_b)\,(z_s + h - z) \tag{13}$$

In this, λ = numerical parameter; and z_b and z_s are characteristic lengths determined at z = 0 and z = h, respectively. The characteristic lengths z_b and z_s are very small compared to h and are a measure of the thickness of the viscous sublayer. Eq. (13) very close to the moving and stationary boundaries reduces to,

$$\frac{\nu_t}{u_{*_s}} = \lambda\,(z + z_b) \approx \lambda z_b \quad at \quad z \approx 0 \quad \text{and} \quad \frac{\nu_t}{u_{*_s}} = \lambda\,(z_s + h - z) \approx \lambda z_s \quad at \quad z \approx h \tag{14}$$

Eq. (14) indicate that the characteristic lengths vary linearly with distance from the boundaries. The ratio between the bottom and surface characteristic lengths and shear stresses are assumed to be related as follows, $z_b u_{*_b} = z_s u_{*_s}$ or in terms of η

$$z_b = z_s\,|\,\eta|^{-0.5} \tag{15}$$

Using the nondimensional variables, $z_{bh} = z_b/h$, $z_{sh} = z_s/h$ and $\bar{u}_o = \bar{u}/u_{*_s}$ in Eq. (7), and with Eq. (13) yields

$$\tau = \rho\,\lambda\, u_{*_s}\,(z_h + z_{bh})\,(z_{sh} + 1 - z_h)\,\frac{d\bar{u}}{dz_h} \tag{16}$$

in which z_h is the nondimensional depth. Further, using the linearity of the shear stress distribution with Eq. (16) yields

$$\frac{d\bar{u}_o}{dz_h} = \frac{\eta + (1-\eta)\,z_h}{\lambda\,(z_h + z_{bh})\,(z_{sh} + 1 - z_h)} \tag{17}$$

which, after intergration, yields the distribution of the mean velocity

$$\bar{u}_o = -\frac{1}{\lambda(1+z_{sh}+z_{bh})}\left[((1-\eta)z_{sh}-\eta)\ln\frac{z_h+z_{sh}}{z_{sh}} + ((1-\eta)z_{bh}+1)\ln\frac{z_{bh}+1-z_h}{z_{bh}+1}\right] \tag{18}$$

The boundary condition at the surface, $z_h = 1$, is $\bar{u}_o = \bar{u}_{os} = u_s/u_{*s}$ Applying this to Eq. (18) gives the surface velocity ratio

$$\bar{u}_{os} = -\frac{1}{\lambda(1+z_{sh}+z_{bh})}\left[((1-\eta)z_{sh}-\eta)\ln\frac{1+z_{sh}}{z_{sh}} + ((1-\eta)z_{bh}+1)\ln\frac{z_{bh}}{z_{bh}+1}\right] \tag{19}$$

The average velocity follows from the integration of Eq. (18) with respect to z_h from 0 to 1, and yields

$$\bar{\bar{u}}_o = -\frac{1}{\lambda(1+z_{sh}+z_{bh})}\left[((1-\eta)z_{sh}-\eta)(1+z_{sh})\ln\frac{1+z_{sh}}{z_{sh}}\right.$$

$$\left. -((1-\eta)z_{bh}+1)z_{bh}\ln\frac{z_{bh}}{z_{bh}+1} + (\eta-1)(1+z_{bh}+z_{sh})\right] = 0 \tag{20}$$

In order to satisfy continuity requirements, the average velocity $\bar{\bar{u}}_{os}$ must be equal to zero. Knowledge of the surface velocity ratio $\bar{u}_{os}$, and the bottom to surface shear stress ratio η makes possible the determination of the mean velocity distribution in the vertical direction through Eqs. (15), (18), (19) and (20). The three unknown z_b, z_s and λ are involved implicitly in Eqs (15), (19) and (20) and can be determined from the solution of these three equations. The mean velocity distribution is realized by using the determined values z_b, z_s and λ in Eq. (18).

Values for the numerical parameter $\lambda = 0.125, 0.175, 0.25, 0.35, 0.60$, and a typical value of the surface velocity ratio $\bar{u}_{os} = 18.0$, are depicted in Figs. 4 and 5. These diagrams show, for different bottom-to-surface shear stress ratios, the velocity distribution normalized by the surface velocity, and the corresponding parabolic eddy viscosity distribution normalized by the surface shear velocity and the depth of flow. Close inspection of the velocity profiles reveals that the surface and bottom characteristic lengths decrease with increasing Reynolds number having similar behaviour with their corresponding viscous sublayers.

The relation between the characteristic lengths and the shear stresses given by Eq. (15) is rather arbitrary and needs verification. The drift current is larger than the return bottom current which suggests a thinner viscous sublayer and larger shear velocity than the corresponding ones at the bottom, i.e. z_{bh} and u_{*b} are smaller in magnitude than the z_{sh} and u_{*s} respectively. It was found by Van Dorn (1953) that the bottom characteristic length z_{bh} is of the order of 10^{-3} to 10^{-4} while Reid (1957) determined in his analysis that z_{sh} has a value around 1/3000. These values are incorporated in this model through the relations $z_s u_{*s} = z_b u_{*b}$, $z_s = z_b$, $z_s u_{*b} = z_b u_{*s}$ which yield the velocity profiles portrayed in Figs. 4, 6 and 7. The change in the relation between these parameters influence mainly the return portion of the flow.

Physical Background of Wind-induced Water Currents

Air-water Interface: The wind acting on the water body surface generates waves and causes a drift current. At low wind velocities, where the wind stress is supported by viscous drag and by the form drag of the capillary waves, the wind drives the surface current directly or through the micro-breaking and viscous dissipation of the capillary waves, in which wave energy is lost to turbulence and eventually dissipated and the corresponding wave momentum enhances the surface current. At higher wind speeds the breaking of gravity waves (whitecaps) adds considerably to the total energy dissipation and contributes to the mixing of the surface waters. Based on field data Stewart (1962) estimated that the momentum flux retained by the waves, the so-called wave drag, i.e., the portion of the wind stress extracted by the increase of wave momentum in the growing phase, is 20% of the total wind stress but becomes 0% as the waves become fully developed, (Donelan 1979). In laboratory tanks due to the short fetch present the waves are steeper than the natural waves and the wave drag is in the range of 30 - 50% of the total wind stress (Goossens et al. 1982).

Surface drift velocity u_{sw} has been measured in the laboratory by Baines & Knapp (1965), Keulegan (1951), Masch (1963), Hellstrom, Forssblad and Holmgren (all mentioned in Reid 1957), Wu (1975), Lin & Gad-El Hak (1984), Tsuruya et al. (1985) and others. Such results are typically presented as a fraction of the mean air speed. The drift velocities were determined by timing the passage of floating sawdust, current meter (Reid 1957), neutrally buoyant particles (Baines & Knapp 1965 ; Keulegan 1951), slightly buoyant spherical particles, thin circular disks (Wu 1975), paper disks (Lin & Gad-El Hak 1984) and thin circular papers punched from computer cards (Tsuruya et al.1985), over a given distance in combined wind and water tunnels. An asymptotic value of 0.033 for the ratio of water surface velocity to mean air velocity with increasing Reynolds number was found by Keulegan (1951). Experiments by Wu (1975) resulted in values of this ratio as high as 0.052 but these were found to decrease with an increase in fetch to an asymptotic value of 0.035. Experiments by Lin & Gad-El Hak (1984) and by Tsuruya et al. (1985) resulted in values of this ratio of 0.032 and 0.038, respectively. The commonly accepted value of the ratio of water surface velocity to wind velocity is about 0.030 (Wu 1975).

Replotting the results for the surface drift velocity obtained by others as a fraction of the wind shear velocity, $u_{*a} = (\tau_a/\rho_a)^{0.5}$ Wu (1973) proposed an approximate ratio $u_{sw}/u_{*a} = 0.55$. In terms of water shear velocity the ratio u_{sw}/u_{*w} in the laboratory presumes values between 15 and 25 for a wide range of Reynolds number and flow conditions. In the field Reid (1957) proposes a value of 18.2 while experiments in Great Lakes suggest values as high as 24.0 (the surface velocity is taken as 3% of the wind velocity). The bottom to surface shear stress ratio η presumes values between -0.15 to -0.07 in the previous laboratory studies and as low as -0.20 in the field (Donelan 1974).

Laboratory findings of wind-induced currents have been reported by Baines & Knapp (1965), Goossens et al. (1982), Koutitas & O'Connor (1980), Masch (1963), Lin & Gad-El Hak (1984), Tsuruya et al. (1985) and others. All of these investigations were conducted in air-water tunnels of rectangular cross section and uniform depth. A photographic method using spherical shaped particles as tracers (Baines & Knapp 1965), laser doppler velocimetry (Goossens et al. 1982) and (Koutitas & O'Connor 1980), hot-film anemometry (Tsuruya et al. 1985), and an array of X-film probes (Lin & Gad-El Hak 1984), were used for mean velocity measurements.

Distributions of mean velocity, normalized by the surface velocity u_{sw}, determined in some of the above mentioned experiments are compiled in Fig. 8. The various centre-line profiles do not coincide with each other and the discrepancies are due to differences in Reynolds number, roughness of the air-water interface and unequal drift to return current volume fluxes (the volume flux of the drift current is about 70% of the flux of the return current (Baines & Knapp 1965)). In order to overcome some of the above described shortcomings of the conventional models, a new approach for simulating wind-induced currents is used in this study.

Experimental Apparatus

An existing experimental facility (Audin & Leutheusser 1979), consisting of a moving box propelled by the carriage of a towing-channel installation, and a fixed stationary bench, was modified to meet the needs of the present simulation (Tsanis 1986). In this facility, the moving wall is propelled by the carriage of the towing-tank installation (maximum velocity of 3 m/s) and the fixed wall is the surface of a stationary bench which is constructed alongside the towing channel.

For the purpose of the present investigation, the moving wall of the existing facility is closed on all sides with plexiglass plates, thus forming a moving box. Clearances between box sidewalls and the stationary bench are closed by flexible seals to prevent the air from escaping and keeps the box pressurized during its motion. The moving box is a 2.40 m long and 0.95 m wide pi-shaped plexiglass. The depth of the box, and its inclination relative to the stationary wall can be adjusted between a minimum of 0.01 m and a maximum of 0.15 m. The maximum attainable Reynolds number R_s with u_s = 3.0 m/s and h = 0.15 m is 30000. The stationary wall is 31 m long and begins and terminates 14.5 m away from the two end points of the 60 m long towing channel. The required distances for accelerating and decelerating the carriage to and from its maximum velocity of 3 m/s are less than 14.5 m. Based on this, the whole 31-m length of the stationary bench is available for testing purposes under steady state conditions over the whole range of carriage velocities. For the case of fully established flow of interest herein, the final 10 m of the box travel over the stationary wall were used for testing purposes.

The schematics of experimental equipment used in the present work are depicted in Fig. 9. The velocity and the position of the towing carriage, and the speed of the 2-D traversing mechanism is determined by using interrupt and reflector type optical switches. Flow properties are measured with standard hot-wire velocimetry equipment and guided by the smoke wire-technique used for flow visualization. Single wire probes are used for measuring the velocity. The hot-wire probe can be moved vertically and horizontally by means of a sweep drive unit and a 2-D traversing mechanism, respectively. A DC-component to the turbulent signal is provided by moving the probe horizontally in the region of flow reversal to avoid rectification. The calibration of the hot-wire sensors is done by means of the carriage itself. Details for the calibration of the hot-wire sensors, the smoke-wire technique and data acquisition can be found in Tsanis (1986).

Results and Discussion

A total of seven velocity traverses for different Reynolds numbers between 2000 and 20000 were performed and presented together with the experimental data by Huey & Williamson (1974) and the analytically obtained mean velocity profiles based on a parabolic distribution of the eddy viscosity, in Fig. 10. The theoretically predicted curves are based on a surface velocity ratio of 18.0, while the experimental data for Reynolds numbers of 3000, 5000, 8000, 38600 and 109200 have surface velocity ratios of 15.63, 16.91, 17.92, 21.29 and 23.60, respectively, which are shown in Fig. 11 together with other laboratory and field results. The ratio $\bar{u}_{os}$ appears only in Eq. (19) where it is multiplied by a constant λ. Thus, after matching the experimental profiles with the theoretical predictions, and taking into account the variation of the surface velocity ratio, the empirical relation between the constant λ and Reynolds number R_s is obtained, see Fig. 12, which provides a simple method for calculating velocity profiles in turbulent shear-induced flow.

A better presentation of the mean velocity profiles is in terms of the coordinates of the "smooth" inner law of velocity distribution. In Fig. 13, curve (A) represents the viscous sublayer portion of the velocity profile described by $(u_{sw} - \bar{u}_w) / (u_{*s})_w = (h_w - z)(u_{*s})_w / \nu_w$, and curve (B) represents the logarithmic portion of the velocity profile for hydrodynamically smooth condition, described by

$$\frac{u_{sw} - \bar{u}_w}{(u_{*s})_w} = 5.75 \log \frac{(h_w - z)(u_{*s})_w}{\nu_w} + 6.0 \tag{21}$$

The logarithmic portion of the velocity profile for hydrodynamically rough interface condition, is described by

$$\frac{u_{sw} - \bar{u}_w}{(u_{*s})_w} = 5.75 \log \frac{h_w - z}{z_{ow}} + 8.5 \tag{22}$$

if z_{ow} is expressed as equivalent sandgrain roughness (Schlichting 1968). Introduction of the roughness Reynolds number $R_{kw} = (u_{*s})_w \, z_{ow} / \nu_w$ where z_{ow} is the absolute roughness, or roughness length of the water-side of the air-water interface lead to data presentation shown in Fig. 13 by means of curves C_i i=1,2,3,4 parallel to (B), which are plots of the following equation

$$\frac{u_{sw} - \bar{u}_w}{(u_{*s})_w} = 5.75 \log \frac{(h_w - z)(u_{*s})_w}{\nu_w} + 8.5 - 5.75 \log R_{kw} \tag{23}$$

The experimental data lines have values of R_{kw} between 5 and 70. This finding suggests that most of the existing experimental results compiled in Fig. 13 are in the region of transitional roughness.

The roughness length z_{ow} for the water-side shear layer can be calculated from the values of the roughness Reynolds numbers R_{kw}. The calculated roughness lengths from Baines & Knapp's (1965) and Goossens et al. (1982) experiments, and the water surface shear velocities for some of the above experiments are depicted in Fig. 14, together with the data by Wu (1975) on wind-induced drift currents. The surface shear velocities determined by Wu (1975), Baines & Knapp (1965) and Goossens et al. (1982) are in good agreement with each other, but there are small disrepancies in the roughness lengths due to different fetches in which the experiments were performed.

A new presentation of the data by Baines & Knapp (1965) and Goossens et al. (1982) in terms of the coordinates of the "rough" inner law of velocity distribution are depicted in Fig. 15. Curve (A) represents the logarithmic portion of the velocity profile and curve (B) is the upward shift of curve (A) by a value of $(u_{sw} - \bar{u}_w)/(u_{*s})_w = 1.0$ representing the upper limit of the transitionally rough regime for Nikuradse's sand roughness (Schlichting 1968).

The experimental points, being in the transitionally rough regime, are located mainly around the curves (A) and (B) (results by Baines & Knapp (1965) and were corrected for a wave drag equal to 20% of the total shear stress, i.e. reduction in $(u_{*s})_w$ by 10%). Details on the turbulence characteristics of the wind-induced currents in air-water tunnels and with the present approach can be found in Tsanis & Leutheusser (1987).

The experimentally determined mean velocity profiles shown in Fig. 8 were obtained for different Reynolds numbers, and under different characteristics of surface roughness. From Fig. 13 it is apparent that the experimentally examined flows are in the region of transitional roughness in which the value of the von Karman constant κ is not necessarily equal to 0.4. A value of $\kappa = 0.4$ was used in almost all of the numerical models. All of this contributes to the discrepancies between the numerical and experimental mean velocity profiles.

After an assessment of the previous and present experiments, analytical and numerical models, the present model with $\eta = -0.134$ and $\bar{u}_{os} = 21.0$ (the lower and upper values of these parameters are -0.20 to -0.08 and 15 to 25 respectively) and a parabolic vertical eddy viscosity distribution with $\lambda = 0.30$ (center line value of $\nu_t/(u_{*s}h) = 0.075$) is proposed for applications to prototype problems (the same velocity profile can be obtained with the pair $\bar{u}_{os} = 18.0$ and $\lambda = 0.35$). The characteristic lengths z_{sh} and z_{bh} for this case have values of 2.2×10^{-4} and 0.6×10^{-4} which are in agreement with values in previous studies. The corresponding velocity profile and eddy viscosity distribution are shown in Figs. 3 and 8 for comparison. This model is in overall agreement with the previous models but is preferable for its simplicity in that the mean velocity distribution is determined from a simple algebraic equation involving two logarithms. It may be noted that in cases of developing wind-induced currents, i.e. where there exist separate shear layers at bottom and surface, the eddy viscosity distribution is parabolic only in the surface boundary layer, and is essentially constant in the rest of the flow (Goossens et al. 1982).

Conclusions

A comprehensive review of wind-driven water currents was undertaken, considering both the analytical and experimental approaches to the problem. The existing velocity profiles when plotted in terms of the coordinates of the "smooth inner" law of velocity distribution, delegate all of the experiments into the region of transitional roughness. This conjecture is confirmed when the roughness lengths are calculated and the profiles are found to be consistent with the "rough inner" law of velocity distribution. The shortcomings of conventional laboratory air-water systems are identified to be due to uncontrollable surface roughness and three-dimensionality of flow.

A new experimental system was developed and applied to the simulation of wind-induced water currents. In this approach, the actual water body is represented by the air volume contained inside a moving box, and the surface of a stationary wall constitutes the actual air-water interface. This shear-induced flow overcomes many of the problems plaguing the conventional systems, i.e., continuity is better preserved, surface roughness is controllable and measurements of turbulence quantities by hot-wire anemometry become possible.

Results of measurements of mean velocity profiles in steady turbulent shear-induced flow are found to compare very well with the predictions of a new analytical model based on a parabolic distribution of the eddy viscosity which is proposed for prototype applications.

Appendix I. - References

Aydin, M. and Leutheusser H.J. (1979). "Novel experimental facility for the study of plane Couette flow", *Review of Scientific Instruments*, 50(11), 1362-1366.

Baines, W.D., and Knapp, D.J. (1965). "Wind driven water currents", *J. Hydr. Div.*, ASCE, 91(2), 205-221.

Donelan, M., Elder, F.C. and Hamblin, P.F. (1974). "Determination of the aerodynamic drag coefficient from wind set-up (IFYGL)", *Proc. 17th Conference Great Lakes Research*, 778-788.

Donelan, M.A. (1979). "On the fraction of wind momentum retained by waves", *Marine Forecasting*, J.C.J. Nihoul editor, Elsevier Scientific Publishing Company, Amstredam, Netherlands.

Elder, J.W. (1959). "Dispersion of marked fluid in turbulent shear flow", *J. Fluid Mech.*, 5, 544-560.

Ganoulis, J., Koutitas, C. and Tolikas, D. (1980). "Review of in situ measurements and analytical methods for the prediction of the water movement in Thessaloniki bay", *Greek-U.S. Working Conference on Oceanography*, 7-11 July, Egina, Greece.

Goossens, L.T., van Pagee, H.J.A. and Tessel, P.J. (1982). "Vertical diffusion in air driven water flows", *J. Hydr. Div.*, ASCE, 108(2), 995-1009.

Hamblin, P.F. (1987). "Meteorological forcing and water level fluctuations on lake Erie", *J. Great Lakes Res.*, (in press).

Hellstrom, B. (1941). "Wind effects on lakes and rivers", Handligar, *Ingeniors Vetriskaps Akademien*, Nr. 158, Stockholm, Sweden.

Huey, L.J. and Williamson, J.W. (1974). "Plane turbulent Couette flow with zero net-flow", *J. Appl. Mech.*, ASME, 41, 885-890.

Keulegan, G.H. (1951). "Wind tides in small closed channels", *J. Res., Nat. Bur. Stand.*, 46, 358-381.

Koutitas, C. and O'Connor, B. (1980). "Modeling three-dimensional wind-induced flows", *J. Hydr. Div.*, ASCE, 106(11), 1843-1865.

Lau, Y.L. and Krisnappan, B.G. (1981), "Ice cover effects on stream flows and mixing", *J. Hydr. Div.*, ASCE, 107(10), 1225-1242.

Lin, J.T and Gad-El-Hak, M. (1984). "Turbulent current measurements in a wind-wave tank", *J. Geoph. Res.*, 89(C1), 627-636

Masch, F.D. (1963). "Mixing and dispersion of wastes by wind and wave action", *Int. J. Air and Water Pollution*, 7, 697-720.

Pearce, B.R. and Cooper, C.K. (1981), "Numerical circulation model for wind-induced flow", *J. Hydr. Div.* ASCE, 107(3), 285-302.

Reid, R.O. (1957). "Modification of the quadratic bottom-stress law of turbulent channel flow in the presence of surface wind-stress", *Tech. Memor. No. 93*, Beach Erosion Board, U.S. Dep. Army, Washington, D.C.

Rodi, W. (1978). "Turbulence models and their application in hydraulics - A state of the art review", *Technical Report No. SFB 80/T/127*, Univ. of Karlsruhe, Germany.

Schlichting, H. (1968) "Boundary layer theory", McGraw-Hill, New York, N.Y.

Simons, T.J. and Schertzer, W.M. (1986). "Hydrodynamic models of lake St. Clair", *Contribution #86-10*, National Water Research Institute, Burlington, Ontario, Canada.

Stewart, R.W., (1961). "The Wave drag of wind over water", *J. Fluid Mech.*, 10, 189.

Svensson, U., (1978). "Mathematical model of the seasonal thermocline", *Report No. 1002*, Department of Water Resources Engineering, Univ. of Lund, Sweden.

Tsanis, I.K., (1986). "Characteristics of shear-induced countercurrent flow", thesis presented to the University of Toronto, at Toronto, Ontario, Canada, in partial fulfillment of the requirements for the degree of Doctor of Philosophy.

Tsanis, I.K. and Leutheusser, H.J. (1987). "The structure of turbulent shear-induced countercurrent flow", accepted for publication in the *J. Fluid Mech.*, 8 September (in press).

Tsuruya, H., Nakamo, S. and Kato, H. (1985). "Experimental study on wind driven current in a wind-wave tank - Effect of return flow on wind driven current", *The Ocean Surface*, 425-430.

Van Dorn, (1953). "Wind stress on an artificial pond", *J. Mar. Res.*, 12(3), 249-276.

Wu, J. (1973). "Prediction of near-surface drift currents from wind velocity", *J. Hydr. Div.* , ASCE, (ASCE), 99, 1291-1302.

Wu, J. (1975). "Wind-Induced Drift Currents", *J. Fluid Mech.*, 68(1), 49-70.

Appendix II. - Notation

The following symbols are used in this paper:

$c_{1\epsilon}, c_{2\epsilon}$	=	constants;
d	=	width;
g	=	acceleration due to gravity;
h	=	depth of flow;
k	=	turbulent kinetic energy;
L_o	=	dissipation length scale;
l_m	=	mixing length;
R_s	=	bulk Reynolds number;
R_k	=	roughness Reynolds number;
P	=	piezometric pressure;
u, v, w	=	velocity components in, respectively, x, y and z directions;
$\bar{u}_o$	=	velocity normalized by the surface shear velocity;
u_*	=	shear velocity;
x, y, z	=	Cartesian length coordinates;
z_b	=	bottom characteristic length;
z_h	=	length coordinate normalized by flow depth;
z_o	=	absolute roughness, or roughness length;
z_s	=	surface characteristic length;
ε	=	dissipation of turbulent kinetic energy;
η	=	bottom to surface shear stress ratio;
λ	=	numerical constant;

μ	=	dynamic viscosity;
ν	=	kinematic viscosity;
ρ	=	density;
σ_k, σ_ε	=	Prandtl , Schmidt numbers;
τ	=	shear stress; and
τ_{wd}	=	wave drag;

Subscripts

a	=	air;
w	=	water;
s	=	surface;
b	=	bottom.
t	=	turbulent; and
w	=	water;

Superscripts

A prime denotes a fluctuating quantity, and an overbar signifies a temporal mean value.

LIST OF FIGURE CAPTIONS

(a) THE PROTOTYPE

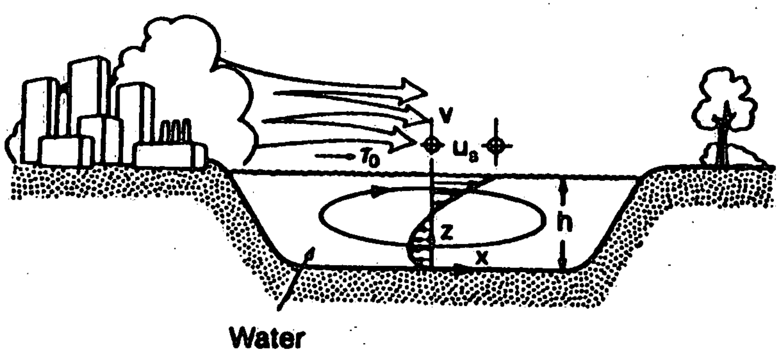

(b) THE MODEL

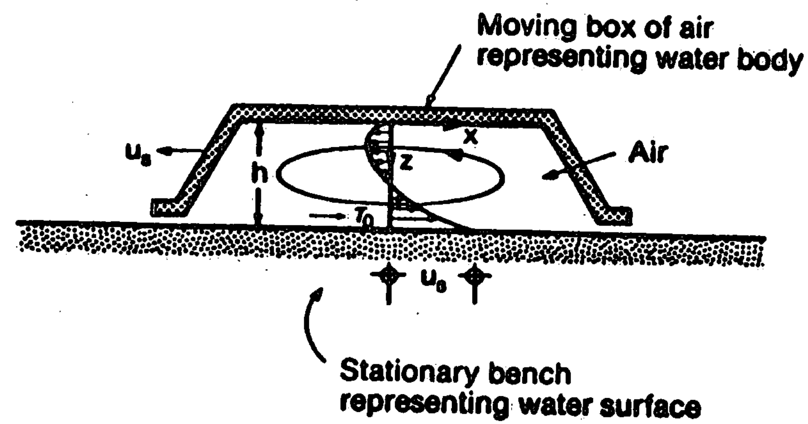

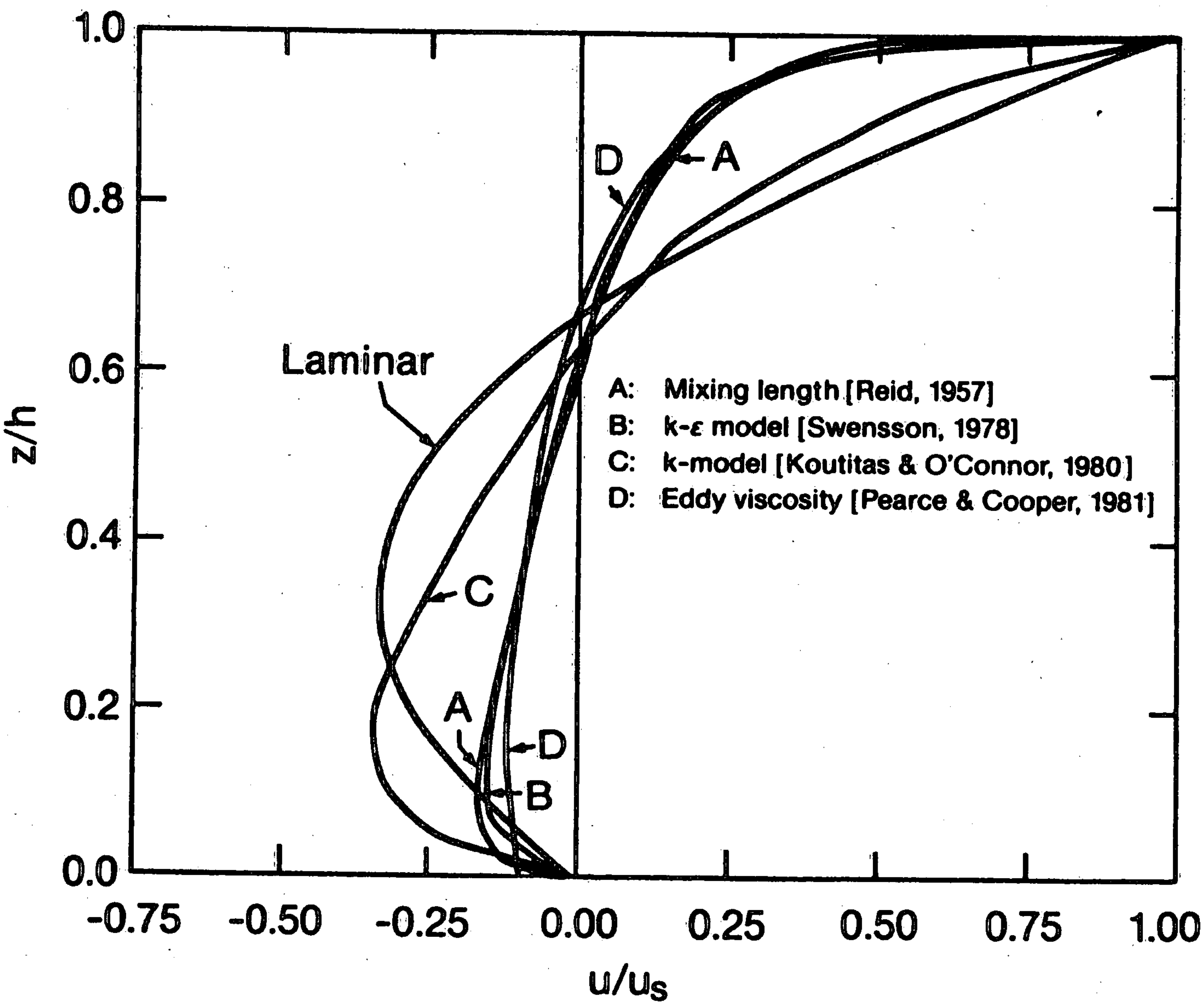

A: Mixing length [Reid, 1957]
B: k-ε model [Swensson, 1978]
C: k-model [Koutitas & O'Connor, 1980]
D: Eddy viscosity [Pearce & Cooper, 1981]
Laminar
A
B
C
D
z/h
u/us

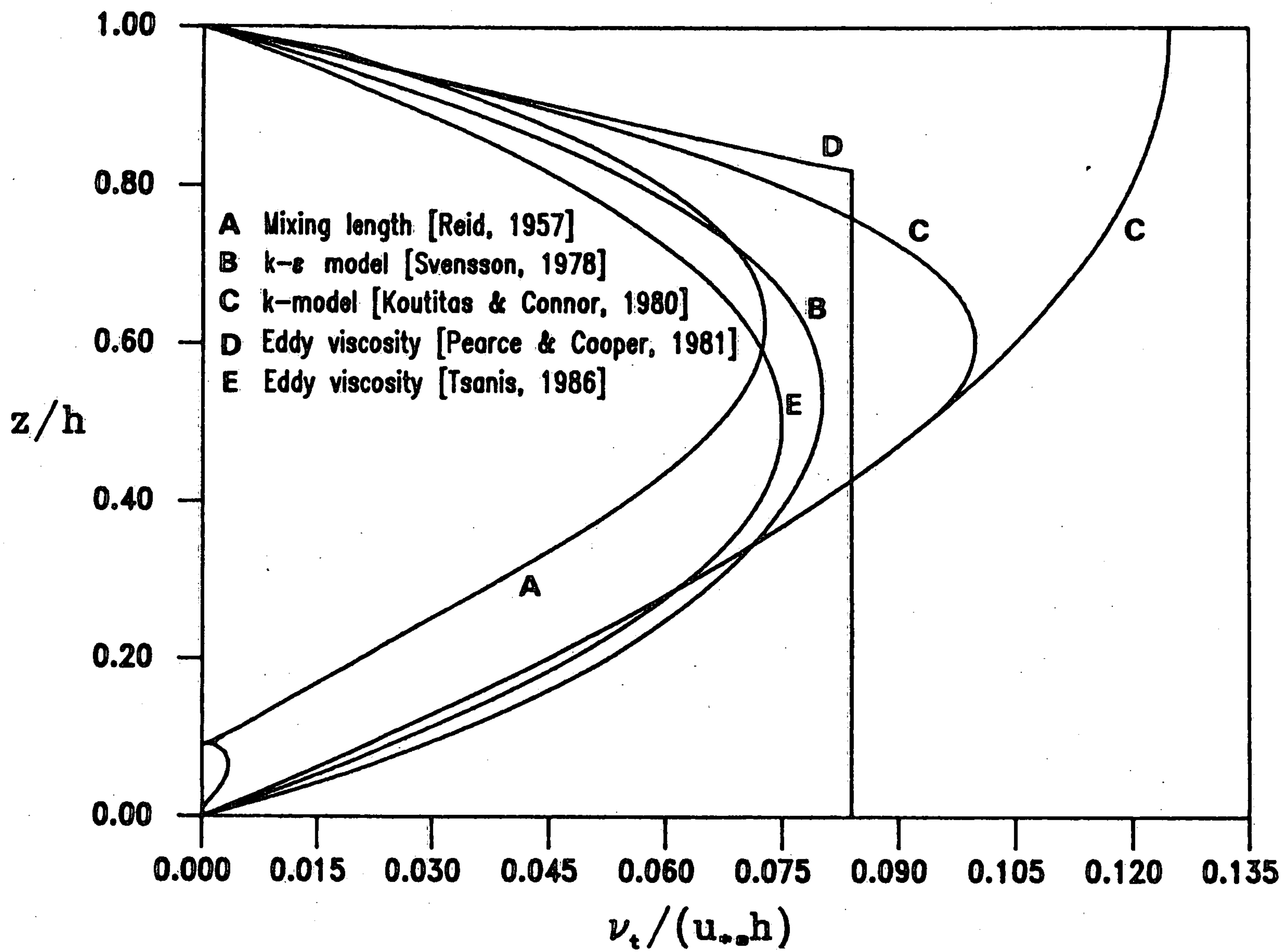

A Mixing length [Reid, 1957]
B k-ε model [Svensson, 1978]
C k-model [Koutitas & Connor, 1980]
D Eddy viscosity [Pearce & Cooper, 1981]
E Eddy viscosity [Tsanis, 1986]
A
B
C
C
D
E
1.00
0.80
0.60
0.40
0.20
0.00
z/h
0.000
0.015
0.030
0.045
0.060
0.075
0.090
0.105
0.120
0.135
ν_t/(u_*s h)

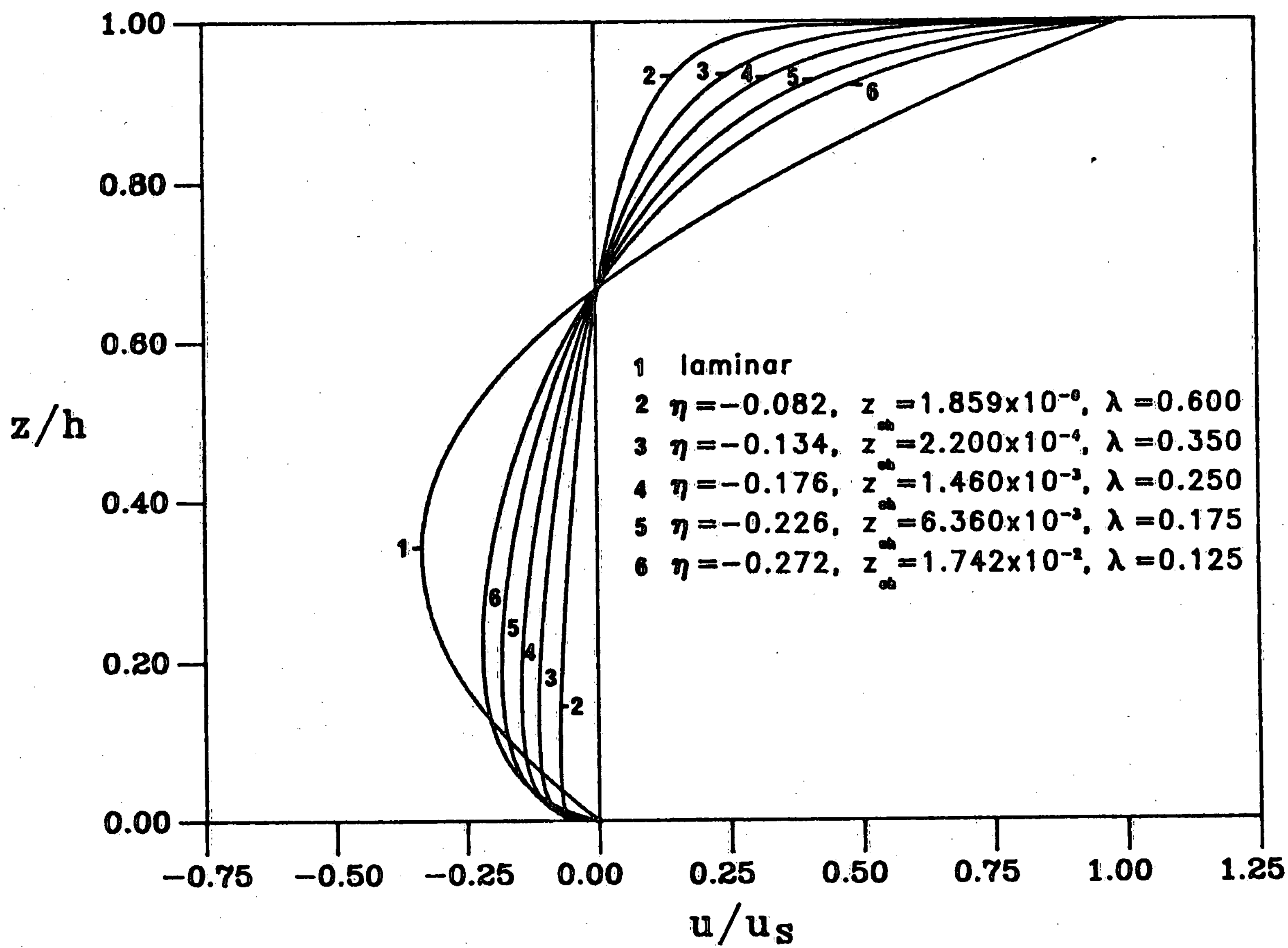

z/h
1.00
0.80
0.60
0.40
0.20
0.00
−0.75
−0.50
−0.25
0.00
0.25
0.50
0.75
1.00
1.25
u/us
1 laminar
2 η=−0.082, z =1.859x10⁻⁶, λ =0.600
3 η=−0.134, z =2.200x10⁻⁴, λ =0.350
4 η=−0.176, z =1.460x10⁻³, λ =0.250
5 η=−0.226, z =6.360x10⁻³, λ =0.175
6 η=−0.272, z =1.742x10⁻², λ =0.125

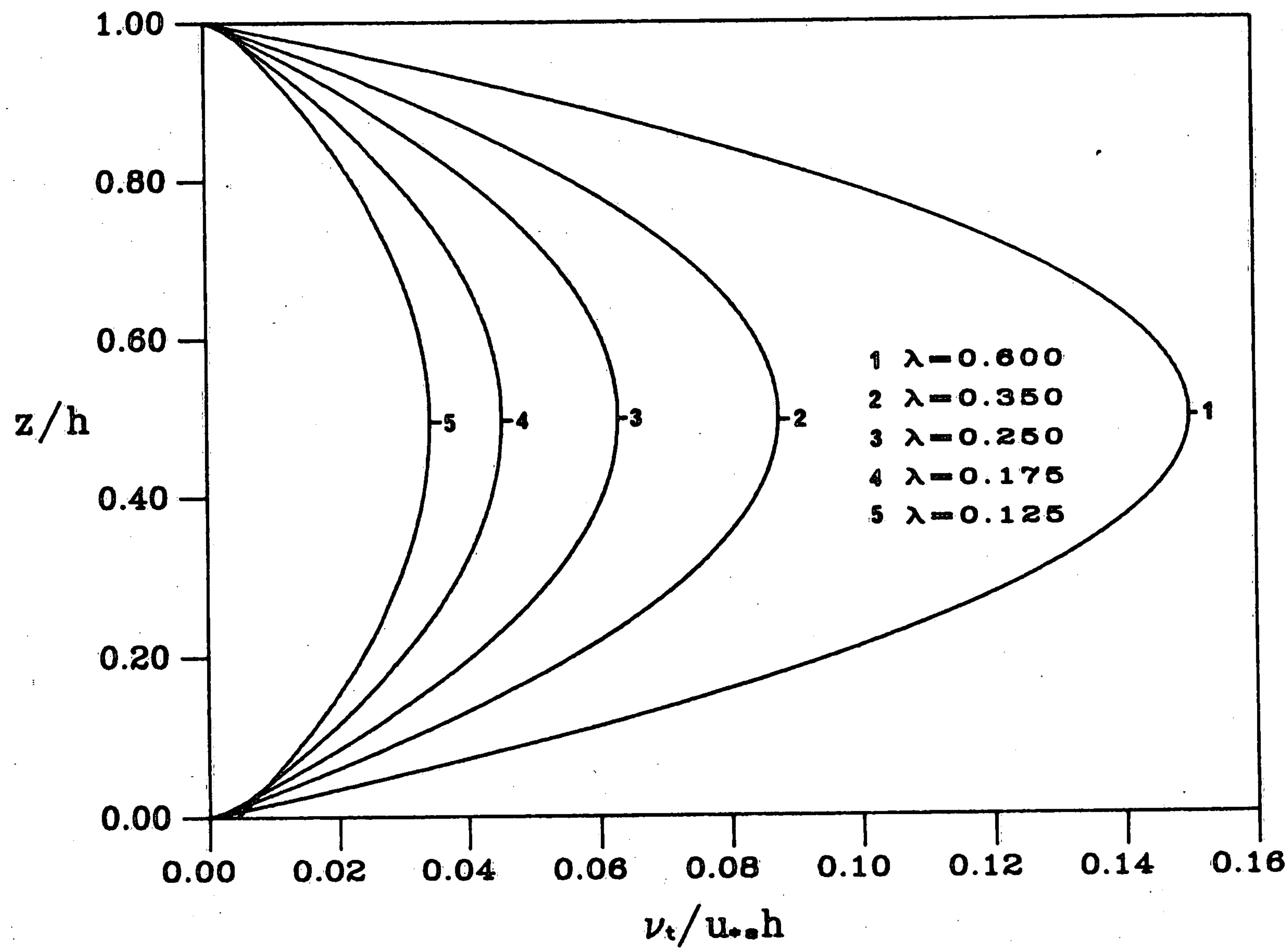
1 λ=0.600
2 λ=0.350
3 λ=0.250
4 λ=0.175
5 λ=0.125
z/h
νt/u*h
1.00
0.80
0.60
0.40
0.20
0.00
0.02
0.04
0.06
0.08
0.10
0.12
0.14
0.16

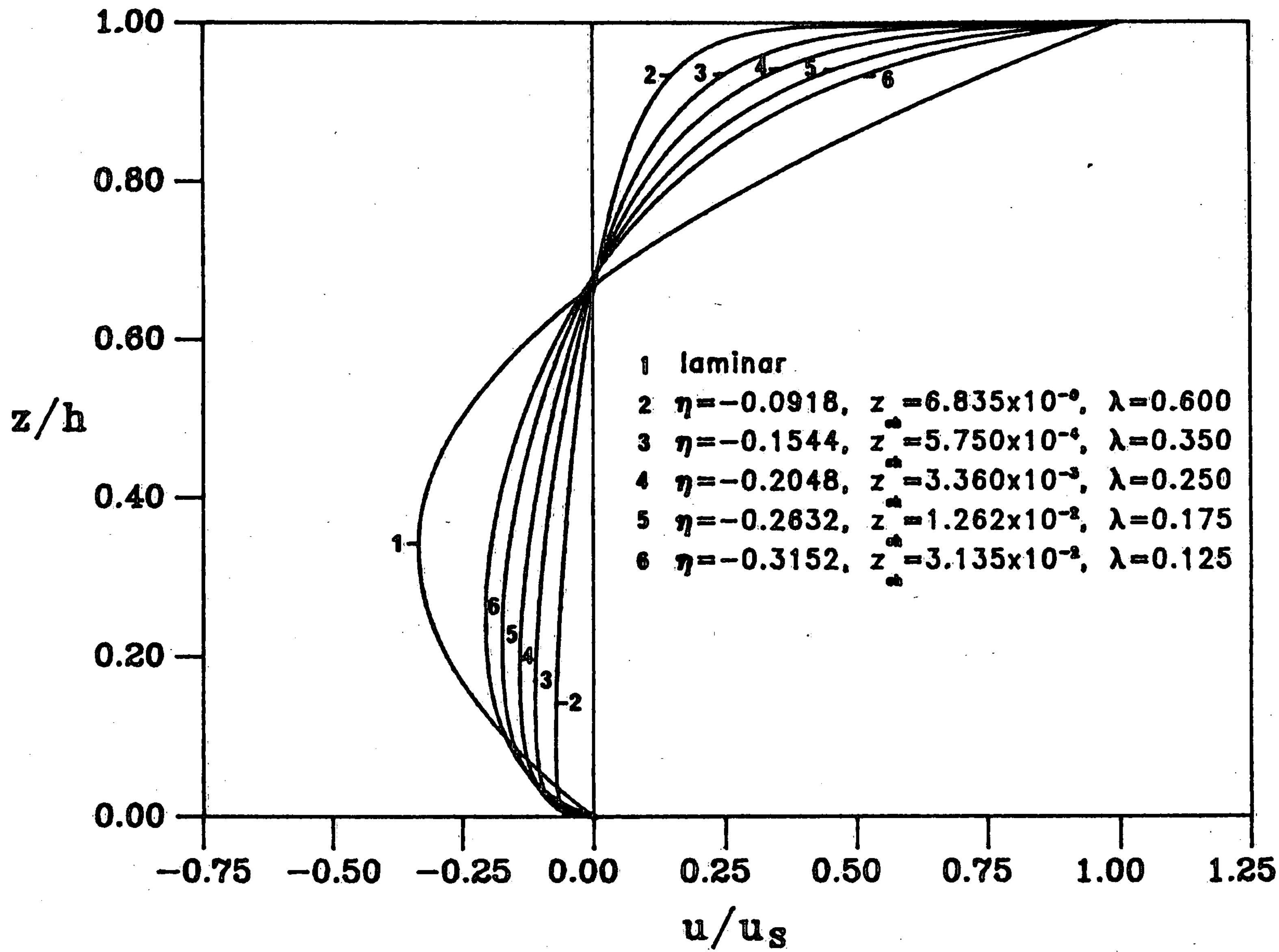
1.00
0.80
0.60
0.40
0.20
0.00
z/h
−0.75
−0.50
−0.25
0.00
0.25
0.50
0.75
1.00
1.25
u/u_s
1
2
3
4
5
6
1 laminar
2 $\eta=-0.0918$, $z_{ob}=6.835\times10^{-9}$, $\lambda=0.600$
3 $\eta=-0.1544$, $z_{ob}=5.750\times10^{-4}$, $\lambda=0.350$
4 $\eta=-0.2048$, $z_{ob}=3.360\times10^{-3}$, $\lambda=0.250$
5 $\eta=-0.2632$, $z_{ob}=1.262\times10^{-2}$, $\lambda=0.175$
6 $\eta=-0.3152$, $z_{ob}=3.135\times10^{-2}$, $\lambda=0.125$

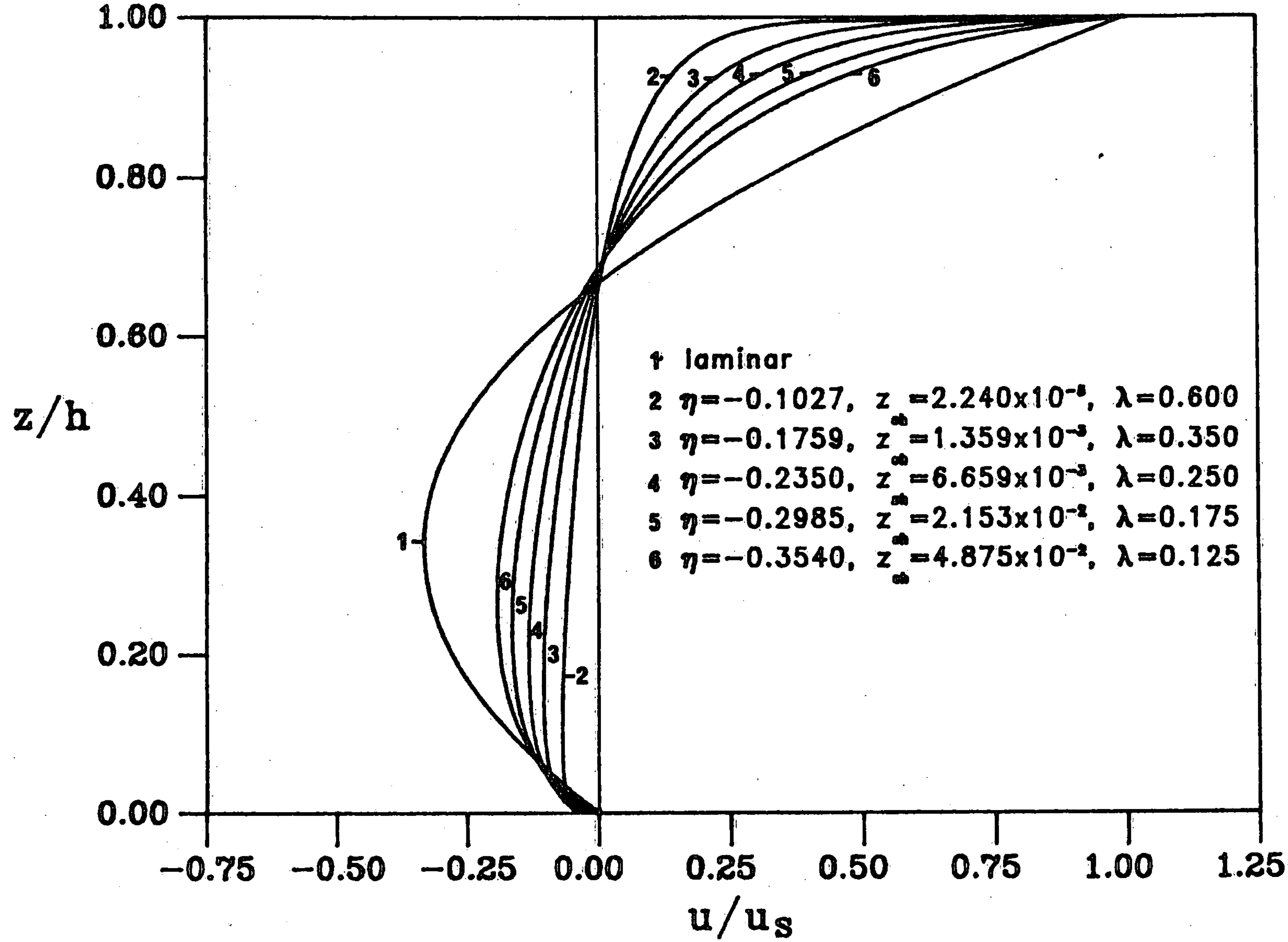

z/h
u/us
1.00
0.80
0.60
0.40
0.20
0.00
−0.75
−0.50
−0.25
0.00
0.25
0.50
0.75
1.00
1.25
1 laminar
2 η=−0.1027, z_{ob}=2.240x10^{-5}, λ=0.600
3 η=−0.1759, z_{ob}=1.359x10^{-3}, λ=0.350
4 η=−0.2350, z_{ob}=6.659x10^{-3}, λ=0.250
5 η=−0.2985, z_{ob}=2.153x10^{-2}, λ=0.175
6 η=−0.3540, z_{ob}=4.875x10^{-2}, λ=0.125

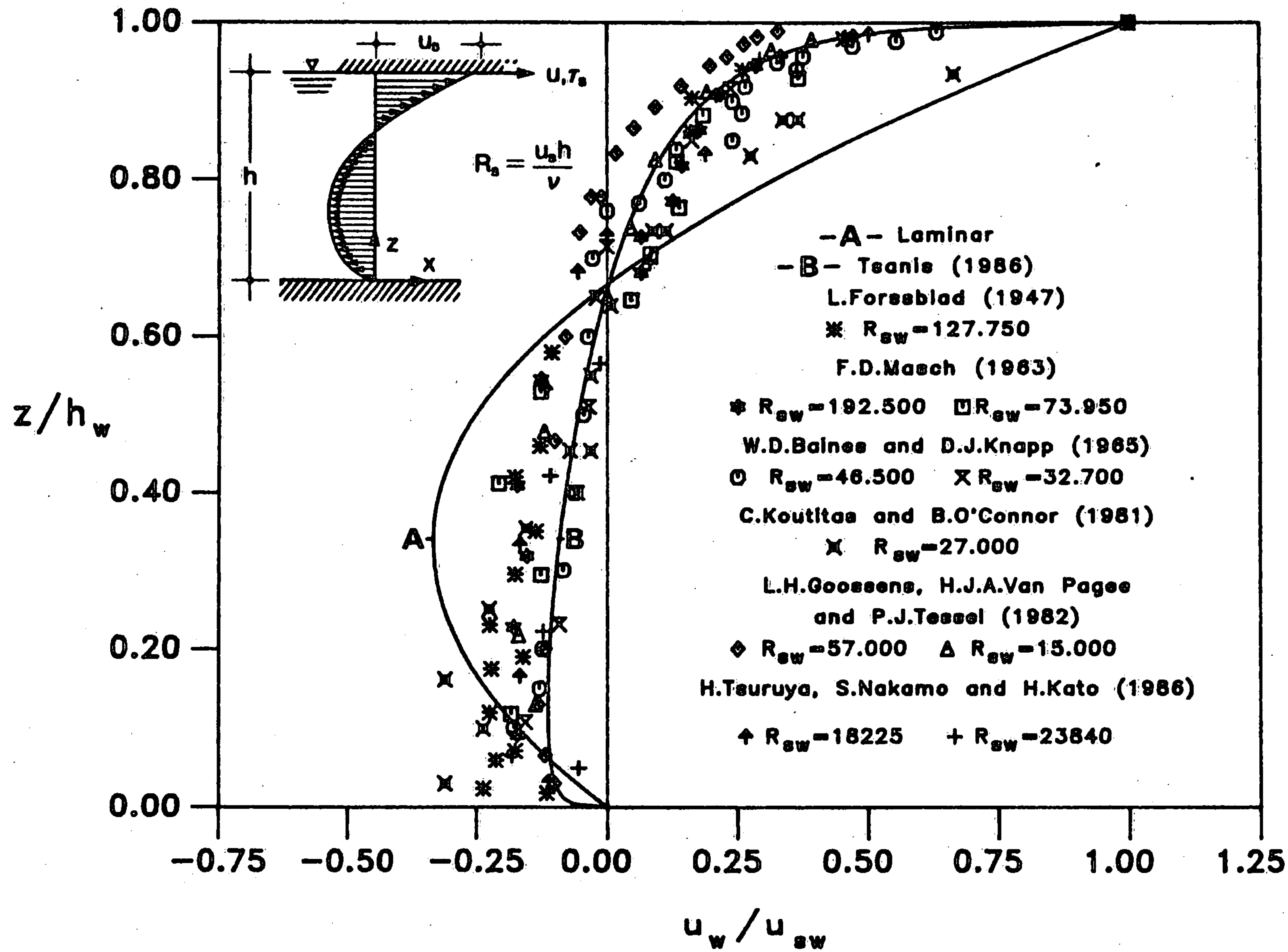

1.00
0.80
0.60
0.40
0.20
0.00
z/h_w
u_s
U, τ_s
h
z
x
R_s = u_s h / ν
A
B
−A− Laminar
−B− Tsanis (1986)
L.Forssblad (1947)
R_sw=127.750
F.D.Masch (1963)
R_sw=192.500 R_sw=73.950
W.D.Baines and D.J.Knapp (1965)
R_sw=46.500 R_sw=32.700
C.Koutitas and B.O'Connor (1981)
R_sw=27.000
L.H.Goossens, H.J.A.Van Pagee
and P.J.Tessel (1982)
R_sw=57.000 R_sw=15.000
H.Tsuruya, S.Nakamo and H.Kato (1986)
R_sw=18225 R_sw=23840
−0.75
−0.50
−0.25
0.00
0.25
0.50
0.75
1.00
1.25
u_w/u_sw

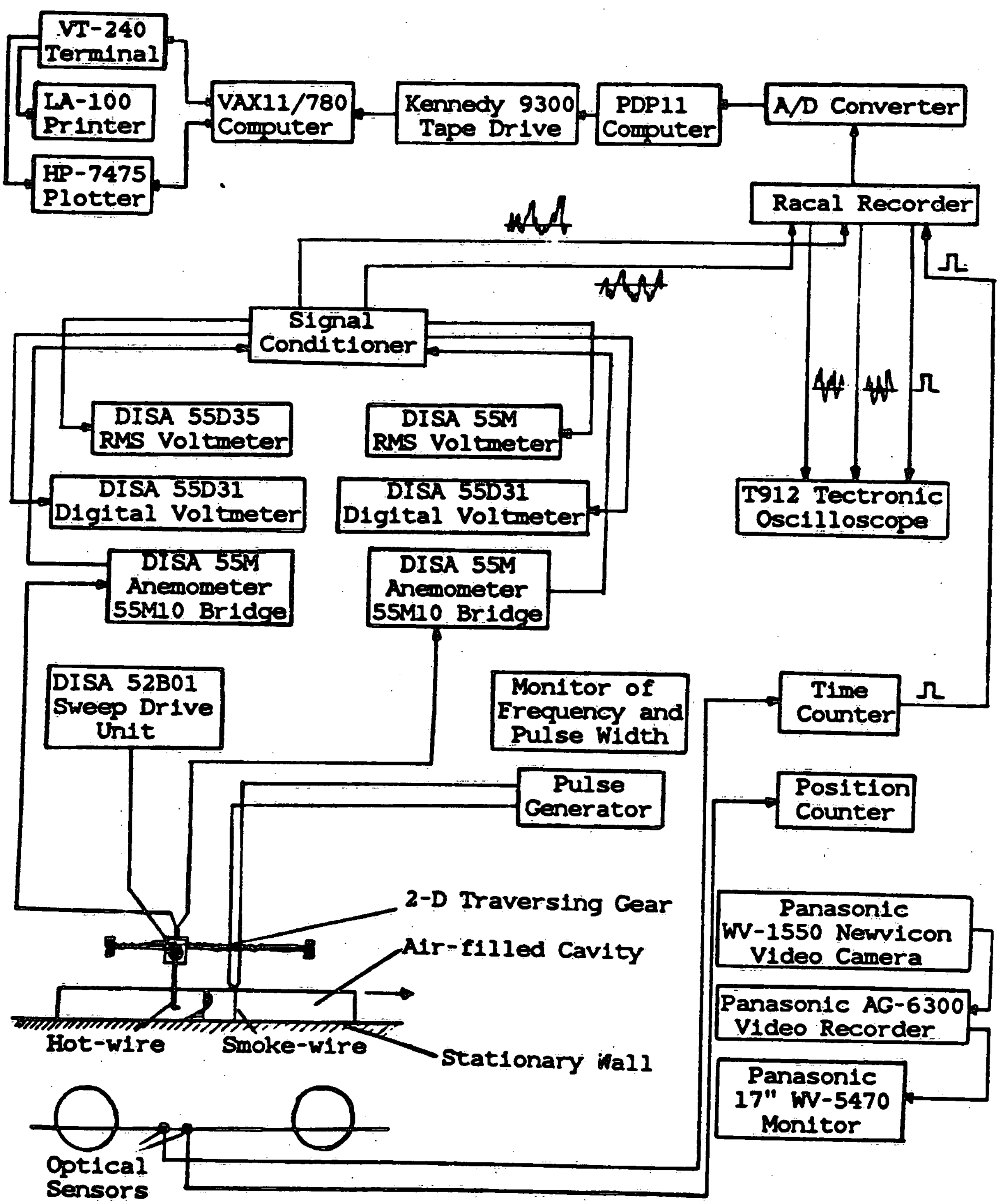
VT-240 Terminal
LA-100 Printer
HP-7475 Plotter
VAX11/780 Computer
Kennedy 9300 Tape Drive
PDP11 Computer
A/D Converter
Racal Recorder
Signal Conditioner
DISA 55D35 RMS Voltmeter
DISA 55M RMS Voltmeter
T912 Tectronic Oscilloscope
DISA 55D31 Digital Voltmeter
DISA 55D31 Digital Voltmeter
DISA 55M Anemometer 55M10 Bridge
DISA 55M Anemometer 55M10 Bridge
DISA 52B01 Sweep Drive Unit
Monitor of Frequency and Pulse Width
Time Counter
Pulse Generator
Position Counter
2-D Traversing Gear
Air-filled Cavity
Panasonic WV-1550 Newvicon Video Camera
Panasonic AG-6300 Video Recorder
Panasonic 17" WV-5470 Monitor
Hot-wire
Smoke-wire
Stationary Wall
Optical Sensors

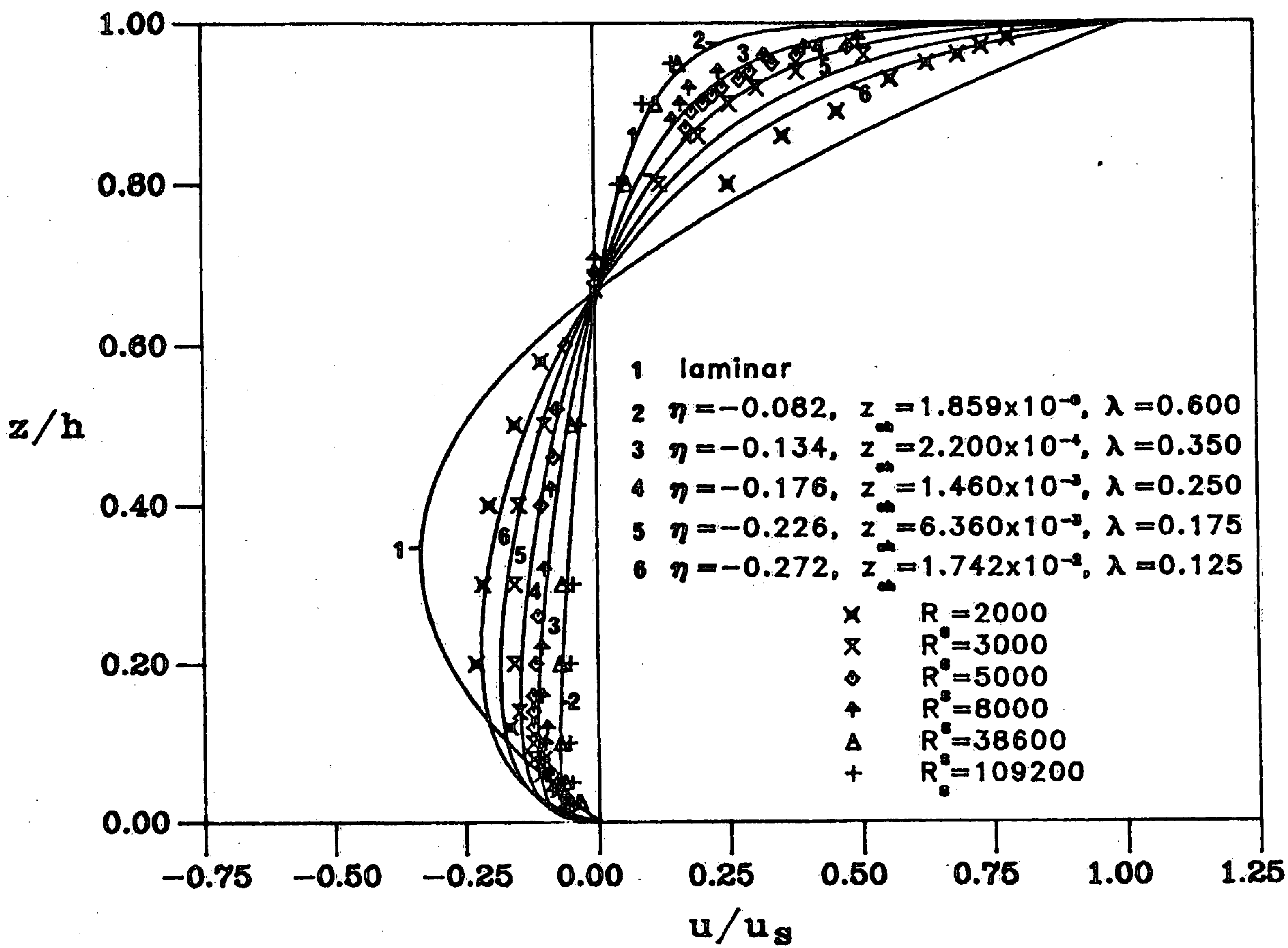

z/h
1.00
0.80
0.60
0.40
0.20
0.00
−0.75
−0.50
−0.25
0.00
0.25
0.50
0.75
1.00
1.25
u/u_s
1 laminar
2 $\eta = -0.082$, $z_{sh} = 1.859\times10^{-6}$, $\lambda = 0.600$
3 $\eta = -0.134$, $z_{sh} = 2.200\times10^{-4}$, $\lambda = 0.350$
4 $\eta = -0.176$, $z_{sh} = 1.460\times10^{-3}$, $\lambda = 0.250$
5 $\eta = -0.226$, $z_{sh} = 6.360\times10^{-3}$, $\lambda = 0.175$
6 $\eta = -0.272$, $z_{sh} = 1.742\times10^{-2}$, $\lambda = 0.125$
$R_s = 2000$
$R_s = 3000$
$R_s = 5000$
$R_s = 8000$
$R_s = 38600$
$R_s = 109200$

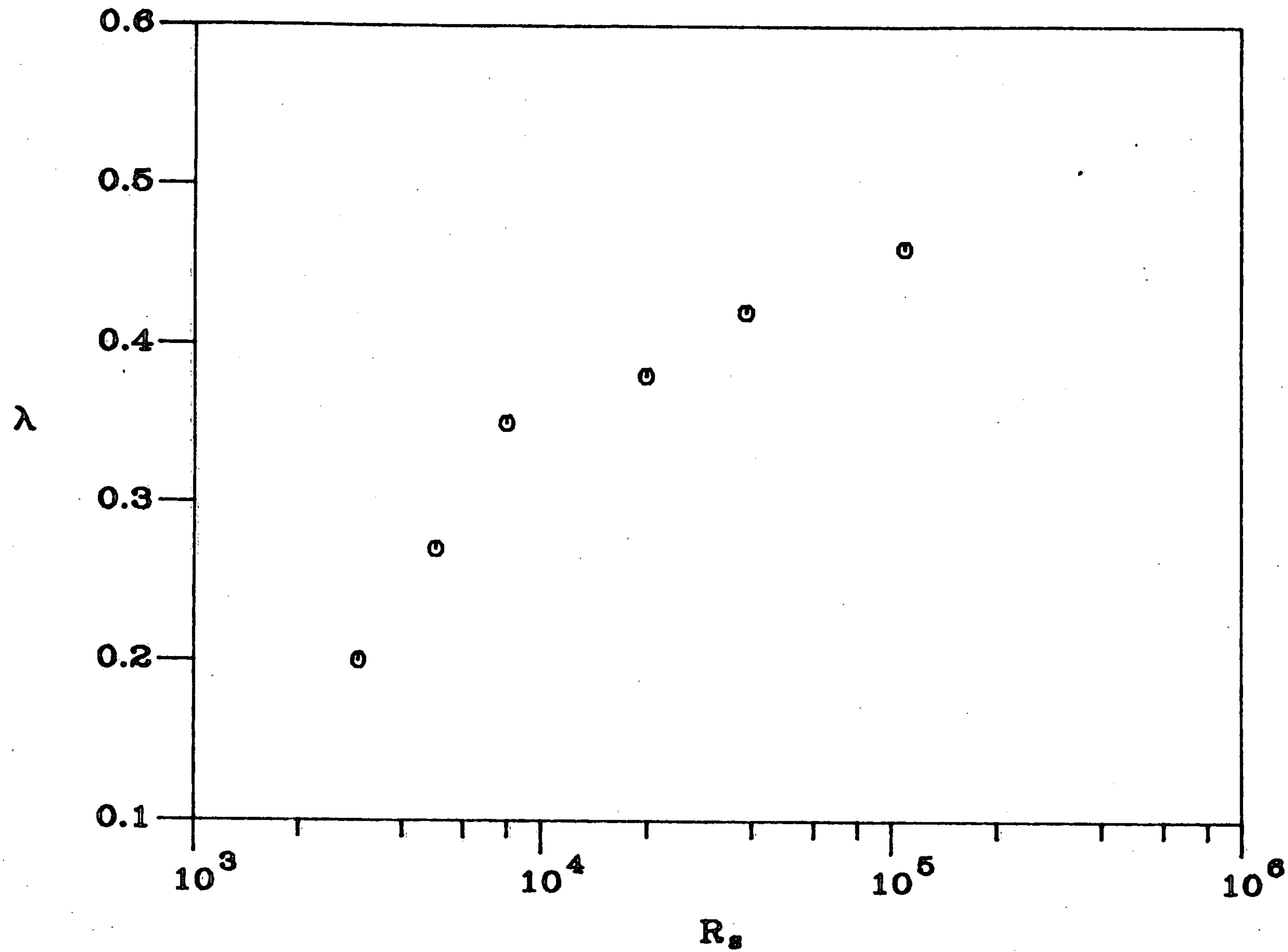
0.6
0.5
0.4
0.3
0.2
0.1
λ
10^3
10^4
10^5
10^6
R_s

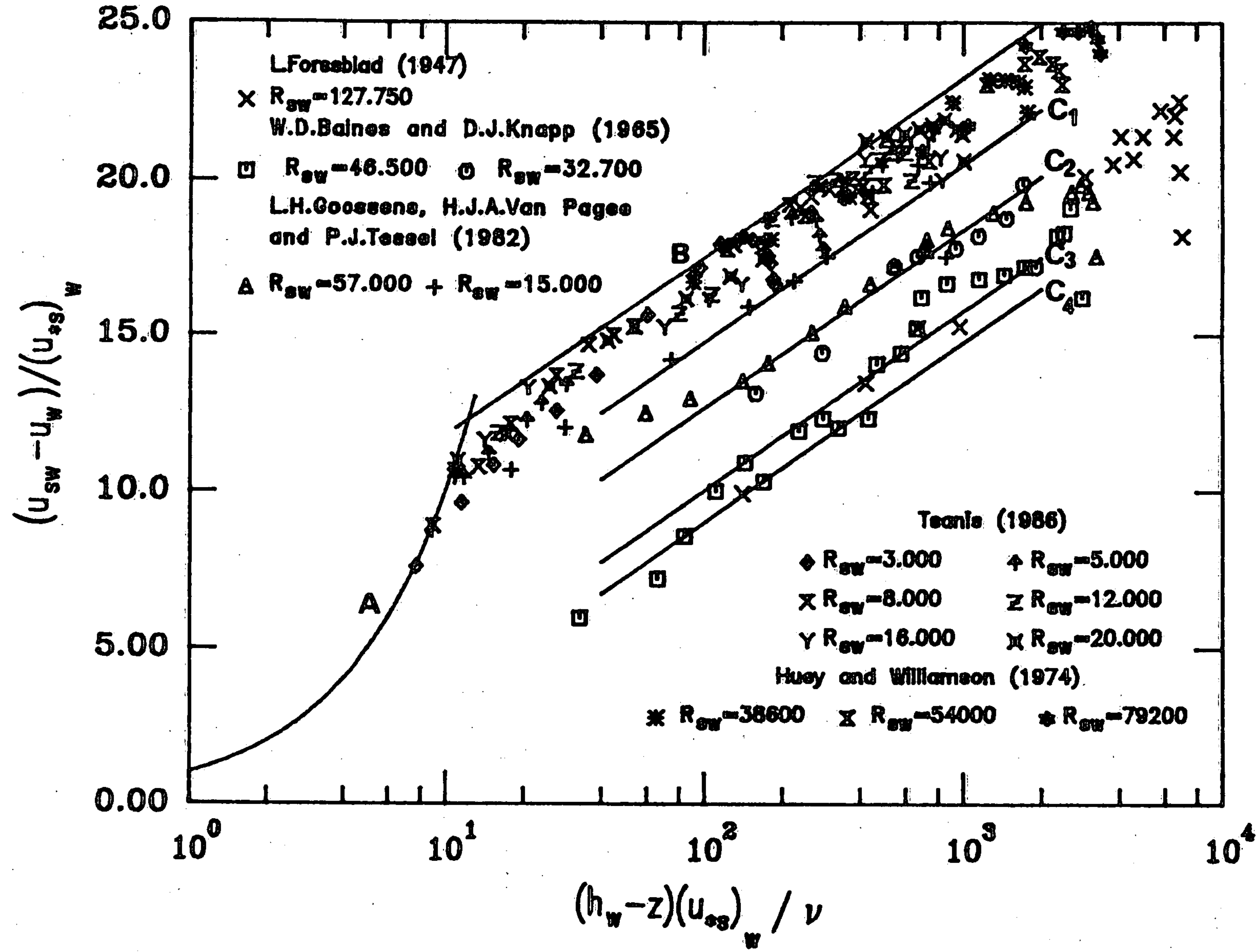

L.Forssblad (1947)
× R_sw=127.750
W.D.Baines and D.J.Knapp (1965)
R_sw=46.500   R_sw=32.700
L.H.Goossens, H.J.A.Van Pagee
and P.J.Tessel (1982)
Δ R_sw=57.000 + R_sw=15.000
Teanis (1986)
R_sw=3.000
R_sw=5.000
R_sw=8.000
R_sw=12.000
Y R_sw=16.000
R_sw=20.000
Huey and Williamson (1974)
R_sw=38600
R_sw=54000
R_sw=79200
A
B
C1
C2
C3
C4
25.0
20.0
15.0
10.0
5.00
0.00
10^0
10^1
10^2
10^3
10^4
(u_sw - u_w)/(u_*s)_w
(h_w - z)(u_*s)_w / ν

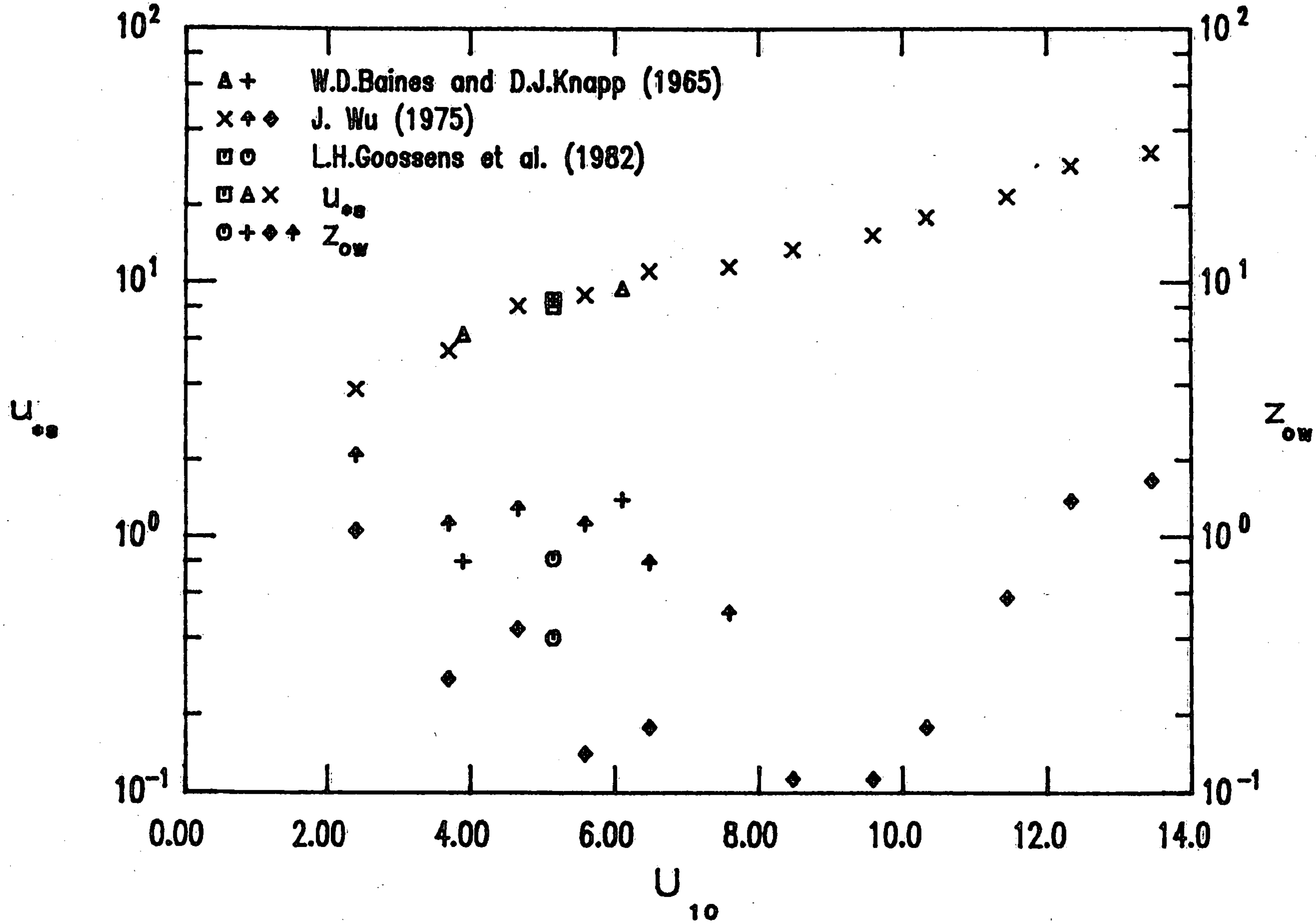
W.D.Baines and D.J.Knapp (1965)
J. Wu (1975)
L.H.Goossens et al. (1982)
u_{**}
Z_{ow}
10^2
10^1
10^0
10^{-1}
0.00
2.00
4.00
6.00
8.00
10.0
12.0
14.0
U_{10}

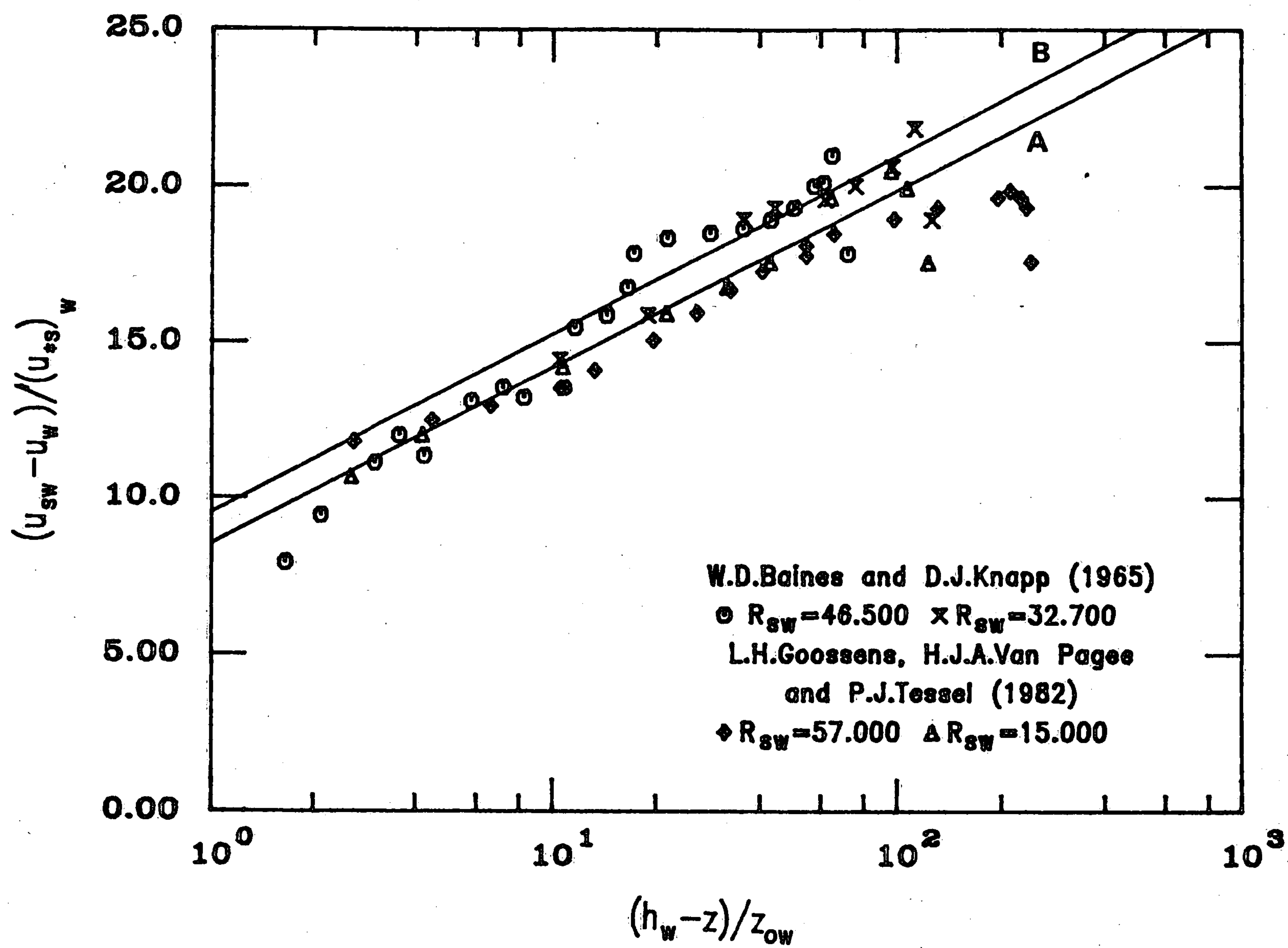
25.0
20.0
15.0
10.0
5.00
0.00
$(u_{sw}-u_w)/(u_{*s})_w$
10^0
10^1
10^2
10^3
$(h_w-z)/z_{ow}$
B
A
W.D.Baines and D.J.Knapp (1965)
R_{sw}=46.500 R_{sw}=32.700
L.H.Goossens, H.J.A.Van Pagee
and P.J.Tessel (1982)
R_{sw}=57.000 R_{sw}=15.000

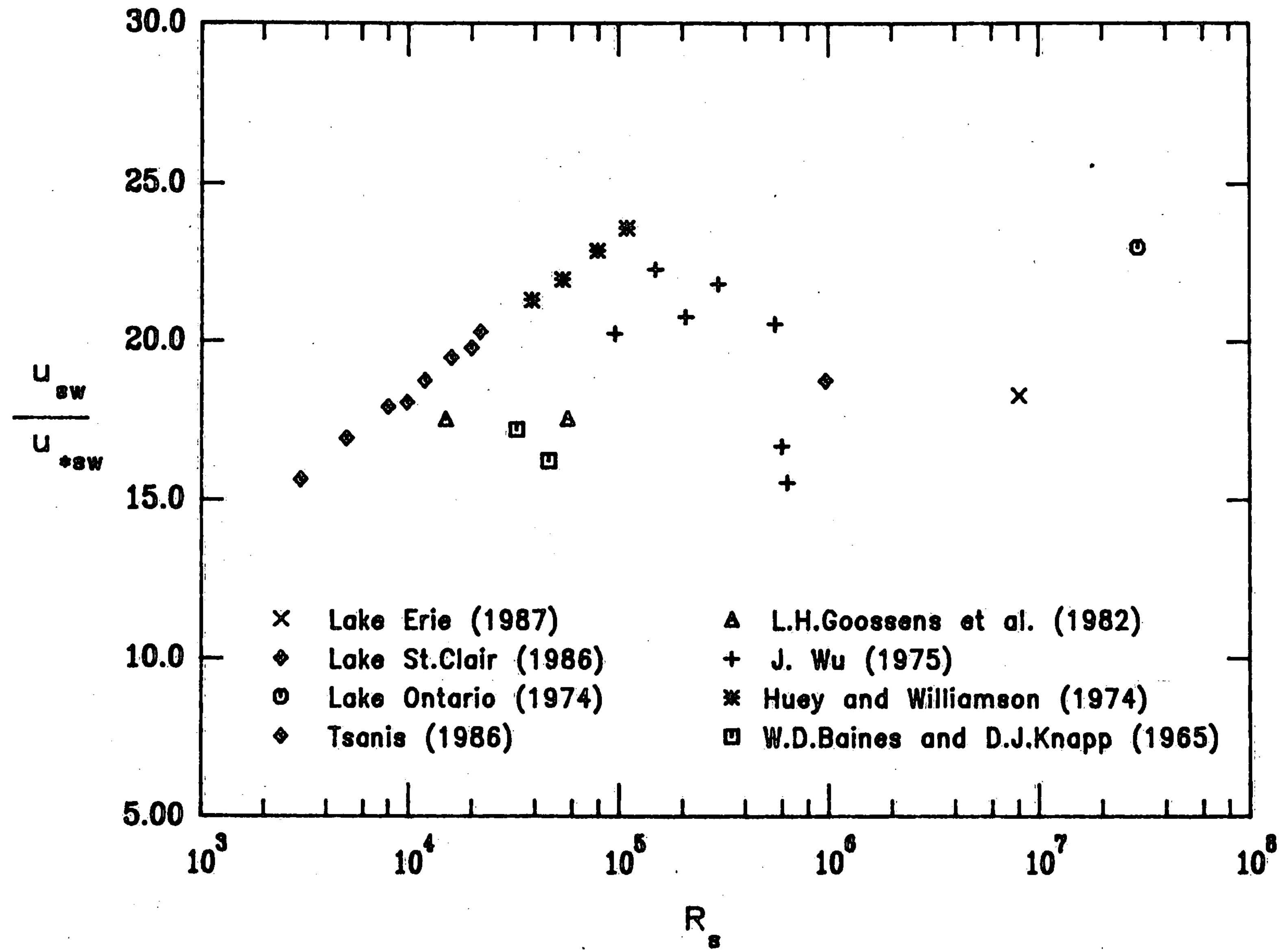

30.0
25.0
20.0
15.0
10.0
5.00
$\frac{U_{sw}}{U_{*sw}}$
10^3
10^4
10^5
10^6
10^7
10^8
R_s
Lake Erie (1987)
Lake St.Clair (1986)
Lake Ontario (1974)
Tsanis (1986)
L.H.Goossens et al. (1982)
J. Wu (1975)
Huey and Williamson (1974)
W.D.Baines and D.J.Knapp (1965)

Paper Reprint Summary

Simulation of wind-induced water currents, by Ioannis K. Tsanis. Analytical and experimental approaches to wind-induced water currents are presented. A novel experimental approach is used to simulate these motions in the laboratory. An analytical solution was found to verify the mean velocity profiles obtained with this apparatus.

Information Retrieval Abstract

SIMULATION OF WIND-INDUCED WATER CURRENTS Ioannis K. Tsanis (Visiting Fellow, National Water Research Institute, Canada Centre for Inland Waters, Burlington, Ontario, L7R 4A6, Canada).

A review of theoretical and conventional experimental approaches to studies of wind-induced water currents is presented. Mean velocity profiles obtained in conventional air-water systems when plotted in terms of the coordinates of the "smooth inner" law of velocity distribution, delegate all of the experiments into the region of transitional roughness. The shortcomings of laboratory air-water systems such as uncontrollable surface roughness and three-dimensionality of flow, are overcome with a novel experimental system. In this approach, the actual water body is represented by the air volume contained inside a moving box while the surface of a stationary wall constitutes the actual air-water interface. Mean velocity profiles obtained with this apparatus are used to verify an analytical solution based on the parabolic distribution of the eddy viscosity.